International Journal of Nanomedicine Dovepress

Open Access Full Text Article ORIGINAL RESEARCH

Toxic Effects of Synthesized Bismuth Oxide/Reduced Graphene Oxide (Bi_2O_3/RGO) Nanocomposites in Two Distinct Mammalian Cell Lines: Role Oxidative Stress and Apoptosis

Rashid Lateef[1,2], Israr Ahmad[2], Abbas Ali Mahdi[3], Neha Lohia[1], Hisham A Alhadlaq[4], Mohd Javed Akhtar[4], Maqusood Ahamed[4]

[1]School of Life and Basic Sciences, Jaipur National University, Jaipur, Rajasthan, 302017, India; [2]Department of Biotechnology, Era University, Lucknow, Uttar Pradesh, 226003, India; [3]Department of Biochemistry, Era University, Lucknow, Uttar Pradesh, 226003, India; [4]King Abdullah Institute for Nanotechnology, King Saud University, Riyadh, 11451, Saudi Arabia

Correspondence: Maqusood Ahamed, King Abdullah Institute for Nanotechnology, King Saud University, Riyadh, 11451, Saudi Arabia, Email mahamed@ksu.edu.sa

Background: Researchers have shown substantial interest in bismuth oxide/reduced graphene oxide (Bi_2O_3/RGO) nanocomposites due to their superior features that are not achievable by each material alone. The growing applications and manufacturing of Bi_2O_3/RGO nanocomposites have raised concerns regarding their potential human health risks. This work was designed to explore the possible toxicity mechanisms of Bi_2O_3/RGO nanocomposites in two distinct mammalian cell lines, normal rat kidney cells (NRK52E) and human liver cancer cells (HepG2).

Methods: Bi_2O_3/RGO nanocomposites were prepared by a simple hydrothermal technique. X-ray diffraction (XRD), transmission electron microscopy (TEM), scanning electron microscopy (SEM), X-ray photoelectron spectroscopy (XPS), and dynamic light scattering (DLS) were used to characterize the synthesized nanocomposites. The cytotoxicity of Bi_2O_3/RGO nanocomposites in NRK52E and HepG2 cells was examined by MTT cell viability assay. Reactive oxygen species (ROS) and glutathione (GSH) were measured as the biomarkers of oxidative stress. The apoptosis study was carried out by measuring several parameters, including cell cycle and caspase-3.

Results: High-quality Bi_2O_3/RGO nanocomposites of ≈33–38 nm size without impurities, where crystalline Bi_2O_3 particles are evenly attached to the RGO sheets. Bi_2O_3/RGO nanocomposites exhibit cytotoxic effects on NRK52E and HepG2 cells, which were dose- and time-dependent. Interestingly, NRK52E exhibited marginally higher vulnerability to Bi_2O_3/RGO nanocomposites compared to HepG2. Bi_2O_3/RGO nanocomposites also cause a dose-dependent increase in ROS production and a decrease in GSH levels. Exposing NRK52E and HepG2 cells to Bi_2O_3/RGO nanocomposites results in activation of the caspase-3 enzyme and chromosomal condensation. The apoptotic response of Bi_2O_3/RGO nanocomposites against both types of cells was further confirmed by AO-EB dual staining and altered cell cycle.

Conclusion: This study demonstrated that the toxicity of Bi_2O_3/RGO nanocomposites in both NRK52E and HepG2 cells is attributed to their ability to produce ROS, leading to apoptosis and cell cycle arrest as a consequence of oxidative stress.

Keywords: Bi_2O_3/RGO nanocomposites, health effects, NRK52E, HepG2, Caspase-3, ROS, apoptosis

Introduction

Nanoscience and nanotechnology are progressively acknowledged for their potential to be applied in almost every aspect of human life, including electronics, energy, agriculture, cosmetics, environmental remediation, and the healthcare systems.[1,2] Nanotechnology enables the creation of novel materials, particles, devices, or structures with at least one dimension ranging from 1 to 100 nm.[3] Nanoscale materials display distinct physicochemical properties in comparison to

Received: 13 September 2024
Accepted: 20 November 2024
Published: 26 November 2024

Graphical Abstract

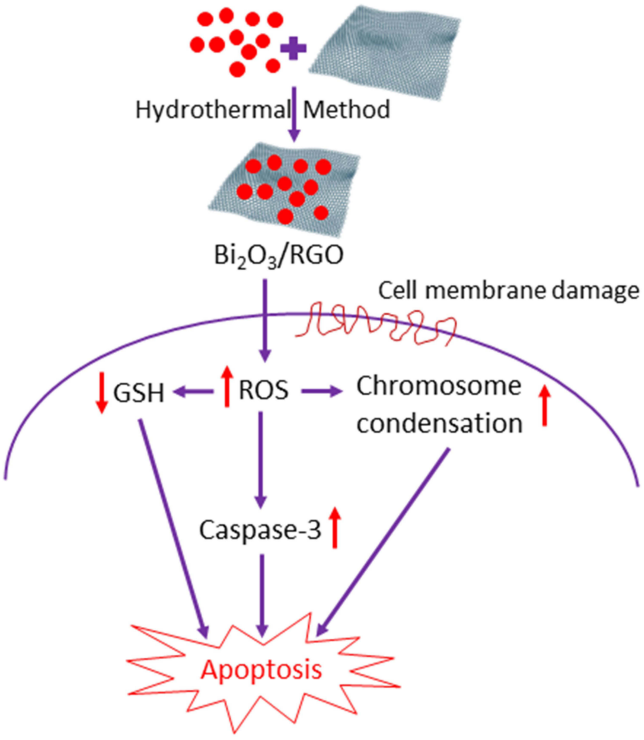

their bulk counterparts. The features of nanoparticles arise from their greater surface area-to-volume ratio. Nanoscale materials are currently a popular subject of research due to their distinctive physicochemical features and their potential for use in diverse applications.[4] Nevertheless, the distinctive attributes of nanoscale materials can potentially have detrimental impacts on environmental and human well-being.[5] Nanoscale materials, due to their smaller size compared to cellular organelles and cells, have the ability to infiltrate fundamental biological structures, potentially causing disturbances to their regular structure and function.[6]

Bismuth oxide (Bi_2O_3) nanoparticles are being exploited for a range of applications, including sensors, paint additives, cosmetics, fuel cells, catalysts, ceramic glasses, microelectronics, and biomedicine, due to their unique optical, electrical, and thermal properties.[7–9] Bogusz[10] developed a theranostic system based on Bi_2O_3 nanoparticles for drug delivery and cancer therapy. Bi_2O_3 nanoparticles have been demonstrated as a promising radiosensitizer in cancer radiation.[11,12] Bi_2O_3 nanoparticles also exhibited a wide range of antibacterial and antifungal properties.[13–15] High-scale production and widespread utilization of Bi_2O_3 nanoparticles could heighten the risk of occupational and environmental exposure to humans. There are some studies that have observed the toxicity of Bi_2O_3 nanoparticles in different mammalian cell lines.[16–18] Bi_2O_3 nanoparticles were also found to generate genotoxicity in the root cells of *Allium cepa* and zebrafish embryos.[19,20]

Graphene consists of a single layer of carbon atoms bonded together in a two-dimensional structure.[21] These carbon atoms are arranged in a way that gives graphene unique features, including high elasticity, flexibility, high conductivity, and the ability to easily undergo functionalization.[22] Novel features of graphene have generated significant interest in the fields of synthetic biology and nanomedicine.[23] Although graphene has significant potential in biomedical applications, its unaltered form exhibits limited solubility in biological fluids, hence complicating the research on nanomedicine in this context.[24] To address this issue, a highly effective strategy has been the utilization of graphene derivatives, specifically graphene oxide (GO) and reduced graphene oxide (RGO). The oxidation process of graphite can be used to synthesize GO, while RGO is the reduced form of GO.[25] The GO and RGO demonstrate exceptional dispersibility and stability in

physiological fluids due to the presence of oxygenated functional groups on their surfaces.[26] Despite tremendous biological applications of graphene and its derivatives, there are conflicting findings in the literature regarding their toxicological profiles. Several studies have found that graphene has good biocompatibility, biodegradability, and advantageous effects on cell proliferation and differentiation.[27,28] However, other studies have indicated negative effects of graphene and its derivatives such as physical destruction of cells, oxidative stress, inflammation, apoptosis, and genetic damage.[29,30]

Graphene surfaces possess a significant quantity of oxygen functional groups and surface imperfections, rendering them advantageous for combining with metal oxide materials (such as ZnO, CeO_2, and Bi_2O_3) to create nanocomposites.[31] Metal oxides and graphene-based nanocomposites displayed fundamentally superior biological properties that could not be attained by a single composition.[32,33] Recent research has found that Bi_2O_3/RGO nanocomposites have improved performances in lithium-ion batteries, supercapacitors, and photocatalytic degradation.[7,34] The Bi_2O_3-based nanocomposite has also shown great potential as an antimicrobial agent, theranostic agent, and efficient radiosensitizer for the eradication of radioresistant tumor.[34–36] The increasing utilization and production of Bi_2O_3/RGO nanocomposites raises concerns regarding their environmental and human health consequences. Comprehensive studies on the possible health risks associated with these nanocomposites are required to establish their suitability for implementation in a wide-spread application such as biomedicine. There is a lack of research on the toxicological effects of Bi_2O_3/RGO nanocomposites.

The Bi_2O_3/RGO nanocomposites can enter the human body through inhalation, cutaneous contact, or ingestion.[37] The kidney, lung, nervous system, and liver are organs that are susceptible to the accumulation and toxicity of nanoscale substances after they enter the body through any of the probable routes of exposure.[38] Hence, such nanostructures could affect most of the vital organs of the human body. Therefore, it is critical to examine the toxicity of nanostructures in pertinent mammalian cell lines.[39,40] The objective of this study was to investigate the mechanism of toxicity of Bi_2O_3/RGO nanocomposites in normal rat kidney (NRK52E) and human liver cancer (HepG2) cells. We have selected two distinct cell types, NRK52E and HepG2 cells, which are often utilized as in vitro models, to investigate the toxicological impacts of Bi_2O_3/RGO nanocomposites. The NRK52E cell line is a stably immortalized cell line derived from rat kidney tubules. The NRK52E cell line has been characterized as an appropriate model for investigating the impact of various xenobiotics or nanomaterials on nephrotoxic damage and mechanistic toxicity.[41,42] We also examined the effects of Bi_2O_3/RGO nanocomposites in HepG2 cells in order to avoid cell-type-specific responses. The HepG2 cell line is derived from the liver hepatocellular carcinoma and is widely utilized for studying the toxicity or impact on hepatocyte function of xenobiotics and/or nanomaterials.[43,44] Bi_2O_3/RGO nanocomposites were prepared using a simple process and characterized by X-ray diffraction (XRD), field emission scanning electron microscopy (FESEM), field emission transmission electron microscopy (FETEM), energy-dispersive X-ray spectroscopy (EDS), dynamic light scattering (DLS), and zeta potential. The MTT assay was used to evaluate the cytotoxicity of Bi_2O_3/RGO nanocomposites in NRK52E and HepG2 cells, considering the dosage and duration of exposure. The investigation of apoptosis in cells exposed to nanocomposites was conducted using parameters such as caspase-3 enzyme, chromosomal condensation, acridine orange-ethidium bromide (AO-EB) dual staining, and cell cycle phases. The toxicity mechanisms of Bi_2O_3/RGO nanocomposites in both cells were investigated by examining the oxidative stress pathway, specifically by measuring the levels of pro-oxidant reactive oxygen species (ROS) and antioxidant glutathione (GSH) in both cell types.

Materials and Methods

Reagents and Chemicals

Dulbecco's modified eagle medium (DMEM), fetal bovine serum (FBS), and antibiotic-antimycotic solution were bought from Invitrogen (Carlsbad, CA, USA). Bismuth(III) nitrate pentahydrate ($Bi(NO_3)_3.5H_2O$, 99.999% trace metal basis), graphene oxide (GO, non-exfoliated), 3-(4,5-Dimethylthiazole-2-yl) 2.5-diphenyltetrazolium bromide (MTT), 2.7-dichlorofluorescin diacetate (DCFH-DA) (≥97% HPLC), 4', 6-diamidino-2-phenylindole dihydrochloride (DAPI, (≥98% HPLC and TLC), acridine orange (AO), ethidium bromide (EB), propidium iodide (PI), and 5.5`-dithiobis

(2-nitrobenzoic acid) (DTNB, (≥98%) were purchased from Sigma-Aldrich (St. Louise, MO, USA). All other chemicals utilized were of the utmost purity and accessible from commercial suppliers.

Synthesis of Bi_2O_3/RGO Nanocomposites

Synthesis of Bi_2O_3/RGO nanocomposites was done by adopting the method of Zhang et al[31] with few specific changes. In brief, 100 mg of bismuth(III) nitrate pentahydrate ($Bi(NO_3)_3.5H_2O$) and 20 mg of GO were introduced into 100 mL of de-ionized water and subjected to ultra-sonication for a duration of 1 h. Subsequently, the mixture was transferred into a Teflon-coated autoclave and allowed to complete the reaction for a duration of 8 h at a temperature of 180°C. Once the product had cooled to room temperature, it was separated by filtration and subsequently washed multiple times with deionized water and ethanol. The nanocomposite was ultimately dried in a vacuum oven at 80°C for 24 h.

Characterization of Bi_2O_3/RGO Nanocomposites

Crystallinity and phase purity of Bi_2O_3/RGO nanocomposites were analyzed using XRD, the PANalytical X`Pert Pro from Malvern Instruments, UK. The FETEM (JEM-2100, JEOL, Inc., Tokyo, Japan) and FESEM (JSM-7600F, JEOL, Inc.) were used to carry out further structural characterizations, including the shape, size, and surface morphology. The elemental analysis was done by EDS. The elemental binding environment of the Bi_2O_3/RGO nanocomposite was analyzed through X-ray photoelectron spectroscopy (XPS) (VG ESCALAB MKII) with a monochromatic AlKα X-ray radiation of 1486.6 eV. Behavior of nanocomposites in aqueous medium (cell culture medium) was studied at DLS and zeta potential from the Zeta-Sizer Nano-HT (Malvern Instruments).

Cell Culture

NRK52E (CRL-1571^{TM}) and HepG2 (HB-8065^{TM}) cell lines were acquired from ATCC (Virginia, USA). The cell lines were cultivated in Dulbecco's Modified Eagle Medium (DMEM), which included high levels of glucose. The medium was supplemented with 10% fetal bovine serum (FBS), 13.5 g/L sodium bicarbonate, and an antibiotic-antimycotic solution consisting of 50 unit/mL penicillin, 50 µg/mL streptomycin, and 0.25 µg/mL amphotericin-B. Cells were grown at a temperature of 37°C in a humidified incubator (90–95% humidity) with a 5% supply of CO_2. When the cell density reached around 85%, the cells were detached from the surface using trypsin and transferred to other flask for further experiments.

Preparation of Stock Suspension and Exposure Protocol

The Bi_2O_3/RGO nanocomposites were dispersed in incomplete DMEM (1 mg/mL of stock suspension). The initially prepared suspension of Bi_2O_3/RGO nanocomposites was further diluted to the desired concentrations, ranging from 1 to 400 µg/mL. Different concentrations of nanocomposites were sonicated for 15 min at a power of 40 W in order to prevent agglomeration before being exposed to cells. Control group is used in each experiment as a comparison to cells using Bi_2O_3/RGO nanocomposites.

MTT Assay

Cytotoxic impact of Bi_2O_3/RGO nanocomposites in NRK52E and HepG2 cell lines was assessed using the MTT test, applying the protocol established by Mossmann[45] with minor adjustments.[46] This assay evaluates mitochondrial function by quantifying the capacity of live cells to convert MTT salt into a blue formazan product. Concisely, 1×10^4 cells were placed in each well of a 96-well plate and treated with Bi_2O_3/RGO nanocomposites at varying concentrations of 1, 5, 10, 25, 50, 100, 200, and 400 µg/mL for 24, 48, and 72 h. Following the completion of the exposure time, the medium was removed from each well to prevent any disruption caused by the nanocomposites during absorbance measurement. It was then substituted with fresh media containing MTT solutions, equivalent to 10% of the culture volume. The samples were kept for 3 h at a temperature of 37°C till formazan product appeared. The formazan crystals were dissolved in dimethyl sulfoxide (DMSO, 100 µL/well). Ultimately, measurement of the absorbance of the solubilized formazan was conducted at 570 nm with the support of a microplate reader (Synergy-HT, BioTek, USA).

ROS Assay

Intracellular amount of ROS in NRK52E and HepG2 cells was quantified after being exposed to Bi_2O_3/RGO nanocomposites. The test was done exploiting the 2.7-dichlorofluorescin diacetate (DCFH-DA) probe, following a method set up by Wang and Joseph[47] with few changes.[46] Two different methods were used to measure the ROS level: a microplate reader was used for a quantitative assay, and fluorescent microscopy was used to observe the fluorescent directly in the cells. To perform the quantitative experiment, 1×10^4 cells were seeded in each well of a 96-well plate with a black bottom. After 24 h, cells were subsequently exposed to nanocomposites (10–200 µg/mL) for 48 h. Following the designated exposure time, the cells were rinsed twice with HBSS and kept in a 1 mL solution of DCFH-DA for 30 min at a temperature of 37°C. Subsequently, the cells were disrupted in an alkaline solution and subjected to centrifugation at 2300 g for a duration of 15 min at ambient temperature. In addition, 200 µL of the liquid remaining after centrifugation was moved to another plate with 96 wells. The intensity of fluorescence was recorded at a microplate reader (Synergy-HT, BioTek) at excitation/emission wavelength of 485/520 nm. Results were presented as a percentage of fluorescence intensity in relation to the controls. An additional group of cells arranged in parallel (3×10^4 cells/well on a 12-well clear plate) were treated with nanocomposites (100 µg/mL for 48 h). Intensity of fluorescence inside the cells was measured using a fluorescent microscope (DMi8, Leica Microsystems).

DAPI Staining for Chromosomal Condensation

The 4', 6-diamidino-2-phenylindole dihydrochloride (DAPI) is a commonly used probe for assessing the nuclei and chromosomes. DAPI produces blue fluorescence when it binds to AT-rich regions of DNA. While the dye is unable to pass through cell membranes, it can still penetrate live cells at larger doses. This study investigated the process of chromosome condensation in NRK52E and HepG2 cell lines due to Bi_2O_3/RGO nanocomposites exposure. The examination was conducted using DAPI labelling, as illustrated earlier.[42] Both cell types were subjected to Bi_2O_3/RGO nanocomposites at a concentration of 100 µg/mL for 48 h. Following the designated exposure time, the control and exposed cells were stained with a 1 mg/mL DAPI solution and incubated in the dark at a temperature of 37°C for 10 min. The nuclei were imaged at a magnification of 20X using a fluorescence microscope (DMi8).

Acridine Orange-Ethidium Bromide (AO-EB) Dual Staining

The apoptosis impact of Bi_2O_3/RGO nanocomposites in NRK52E and HepG2 cells was further analysed using acridine orange-ethidium bromide (AO-EB) dual staining, adopting the process published before.[48] Both cell types were seeded in a 12-well plate and exposed for 48 h to 100 µg/mL concentration of Bi_2O_3/RGO nanocomposites. Cells were rinsed with PBS and further treated with a 2 µL solution containing both AO and EB (100 µg/mL each) (Sigma, USA) for dual fluorescent staining in each well. Subsequently, the brightness of fluorescents in the cells was observed within a time frame of 15 min using a fluorescent microscope (DMi8).

Cell Cycle Analysis

Both cell types were first treated with Bi_2O_3/RGO nanocomposites at a level of 100 µg/mL for 48 h. Then, cells were collected and subjected to centrifugation at 1000 g for 10 min. Collected cell pellets were suspended in 500 µL of PBS. Pellets were then treated with an equivalent amount of ice-cold ethanol (100%) and kept at a temperature of 4°C for 60 min. Following two consecutive PBS washes, the cell pellets were suspended in PBS and treated with a solution containing PI (20 µg/mL), 0.5 mg/mL RNAase A, and 0.1% Triton X-100. The samples were further kept in dark for 30 min at 30°C. The flow cytometer (FACS CantoTM II, BD Biosciences, USA) was employed to quantify PI fluorescence. This was done using a FL4 filter (585 nm), and a total of 1×10^4 events were recorded.[46] Results were examined using Coulter Epics XL/XL-MCL, System II Software, version 3. The investigation excluded cell debris that exhibited a low FSC/SSC characterization.

Preparation of Cell Extract

Cell extract was produced using the methods outlined formerly.[49] Concisely, both cell types (NRK52E and HepG2) were cultivated in a suitable culture flask (eg 25 cm^2) and exposed to varying concentrations (10–200 µg/mL) of Bi_2O_3/RGO nanocomposites for a duration of 48 h. Cells were then collected in ice-cold PBS by gently scratching and subsequently rinsed with PBS at a temperature of 4°C. Cell pellets were subsequently disrupted in a solution called cell lysis buffer, which consisted of 1 × 20 mM Tris-HCl (pH 7.5), 150 mm NaCl, 1 mm Na2EDTA, 1% Triton, and 2.5 mm sodium pyrophosphate. After subjecting the mixture to centrifugal force at 15000 g for 10 min at a temperature of 4°C, the supernatant (cell extract) was collected and stored at 4°C for further experiments. The GSH content and caspase-3 enzyme activity were assayed using the cell extract.

Glutathione Assay

Glutathione (GSH) level in cells was assessed using the method described by Ellman.[50] Concisely, a combination of 0.2 mL of unrefined cellular extract and 1.8 mL of 5% TCA was subjected to centrifugation with a force of 2300 g for a duration of 15 min. Subsequently, 1 mL of the supernatant was combined with 3 mL of a solution comprising 0.01% 5.5`-dithiobis(2-nitrobenzoic acid) (DTNB). The progress of the reaction was observed by measuring the absorbance at 412 nm. GSH concentration was determined in units of nanomole/mg protein.

Measurement of Caspase-3 Enzyme Activity

Caspase-3 enzyme activity assay (colorimetric) kit (#K106) was purchased from BioVision Inc. (Milpitas, CA, USA). This test relies on the fundamental concept that caspases, which are enzymes activated during cell death, cleave artificial substrates to produce a chromophore called p-nitroanilide (pNA). The amount of pNA released is then evaluated at a wavelength of 405 nm. The pNA compound was created using the targeted enzymatic activity of caspase-3 on the tetrapeptide substrate DEVD-pNA.[46] Concisely, the reaction mixture comprised 50 µL cell extract, 5 µL DEVD-pNA (4mM), and 50 µL reaction buffer (2×) containing 10 mm dithiothreitol. This mixture was incubated at 37°C for 60 min. Then, absorbance was measured at 405 nm, as per the instruction of kit.

Protein Assay

The Bradford method was employed to measure the protein level of cell extract.[51] Bovine serum albumin (BSA) was applied as a standard.

Statistical Analysis

All the quantitative results shown in the present work is represented the mean±SD of three separate tests, each test performed in triplicate (n = 3). Statistical assessment was conducted using one-way analysis of variance (ANOVA), followed by Dunnett's multiple comparison tests. The significance was attributed with the p value of <0.05. The Prism application (GraphPad Software, Version 8.0.2, GraphPad Software Inc., San Diego, CA) was employed for all analyses.

Results and Discussion

XRD Study

The XRD pattern of Bi_2O_3/RGO nanocomposites displays the apparent peaks at 2θ of 25.88, 28.14, 30.48, 31.96, 32.86, 41.48, 46.39, 47.10, 51.42, 54.47, 55.67, and 57.94 can be attributed to the diffractions of the crystal planes (210), (201), (211), (002), (220), (212), (222), (400), (123), (203), (421), and (402) (Figure 1). The XRD peaks corresponded to the diffraction peaks of the rhombohedral-phased bismuth planes in the tetragonal structure of β-Bi_2O_3 (JCPDS number. 27–0050).[7] The average size of the crystalline particles in Bi_2O_3/RGO nanocomposites was computed applying the Scherrer`s equation, which involves assessing the FWHM of all the peaks.[52] The mean particle size of Bi_2O_3/RGO nanocomposites was determined to be 39 nm, as shown in Table 1. The presence of sharp and highly intense peaks in the diffraction spectra suggests that the Bi_2O_3/RGO nanocomposites have a high degree of crystallinity. The XRD spectra of

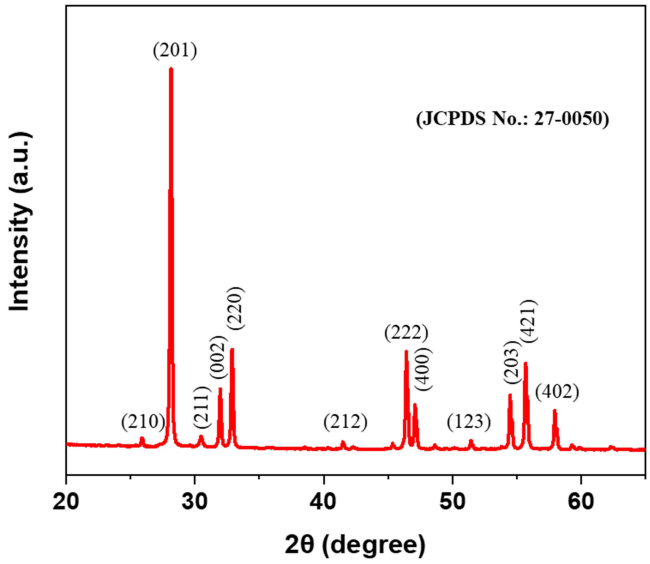

Figure 1 XRD pattern of Bi_2O_3/RGO nanocomposites.

Bi_2O_3/RGO nanocomposites show the absence of a diffraction peak for RGO. This indicates that the dispersion of Bi_2O_3 nanoparticles effectively prevents the RGO sheets from restacking.[53]

SEM Study

The microstructure of Bi_2O_3/RGO nanocomposites was analyzed using FESEM. The SEM micrographs of Bi_2O_3/RGO nanocomposites are illustrated in Figures 2a and 2b. These micrographs demonstrate the presence of spherical nanoparticles firmly attached to RGO sheets. The particle size was determined by computing about hundred particles in randomly selected areas of the SEM picture. Figure 2c displays the particle size distribution derived from the SEM images. The mean particle diameter was determined to be around 33 nm (Table 1). Figure 3a–c depict the elemental mapping of Bi_2O_3/RGO nanocomposites. These figures demonstrate the occurrence of Bi, C, and O components in Bi_2O_3/RGO nanocomposites without impurities. The SEM results are in compliance with earlier studies.[54,55]

TEM Study

The structural analysis of the Bi_2O_3/RGO nanocomposite was further done by FETEM. Figure 4a and 4b depict the standard micrographs obtained from TEM. These TEM images indicate that most of the particles exhibited circular morphology, possessed smooth surface, and evenly attached to the RGO sheets. The presence of creases on RGO sheets suggests that the layers are thin. The particle size distribution of TEM is also displayed in Figure 4c. The average particle size in the nanocomposite was around 37 nm, which is according to XRD and SEM measurements (Table 1). The

Table 1 Physicochemical Characterization of Bi_2O_3/RGO Nanocomposites

Parameters	Mean±SD
XRD size (nm)	38.22 ± 6.54
SEM size (nm)	33.19 ± 14.62
TEM size (nm)	37.04 ± 19.70
Hydrodynamic size (nm)	167.20 ±27.15
Zeta potential (mV)	−9.73±1.6

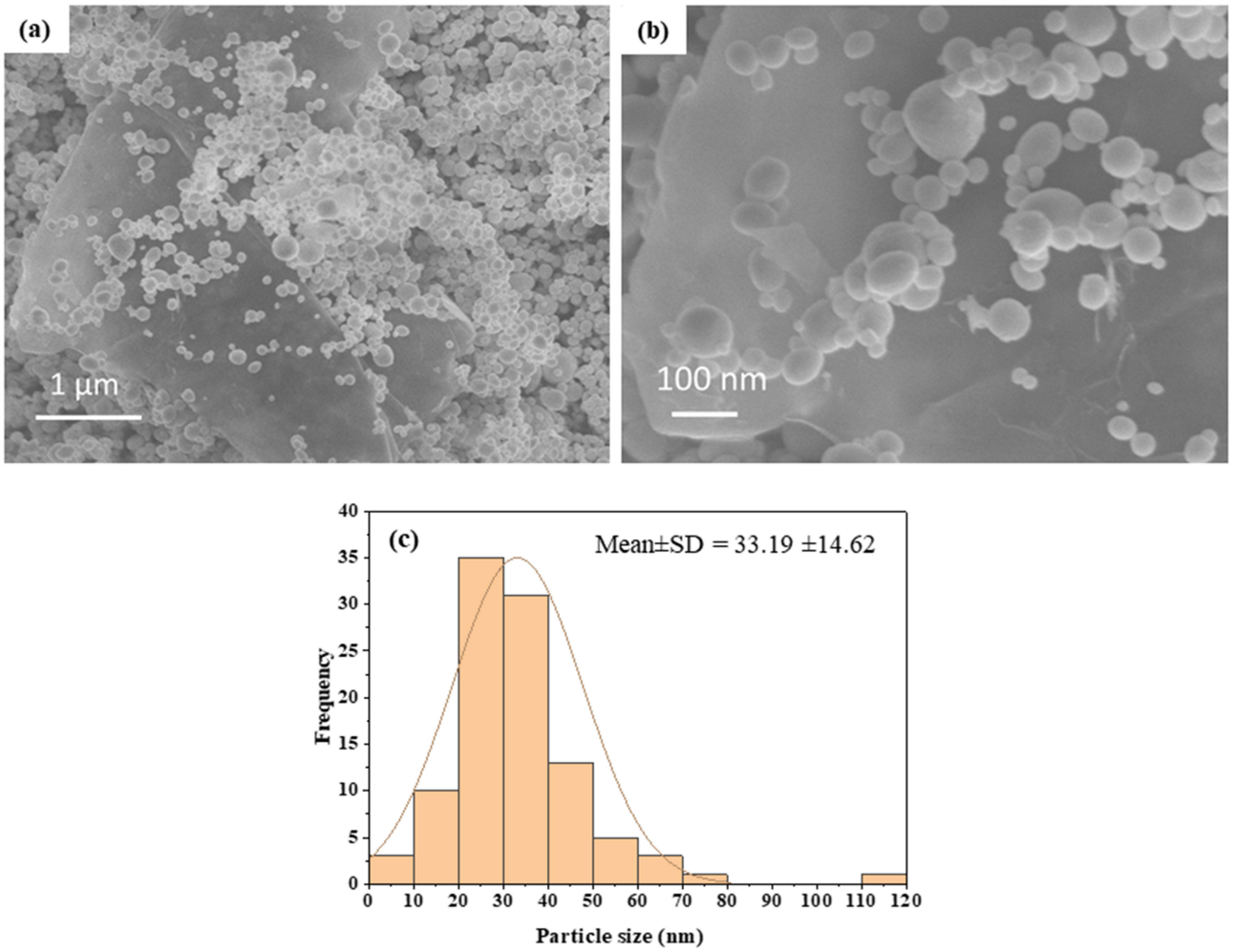

Figure 2 SEM characterization of Bi_2O_3/RGO nanocomposites. (**a** and **b**) SEM micrographs, and (**C**) SEM particle size distribution.

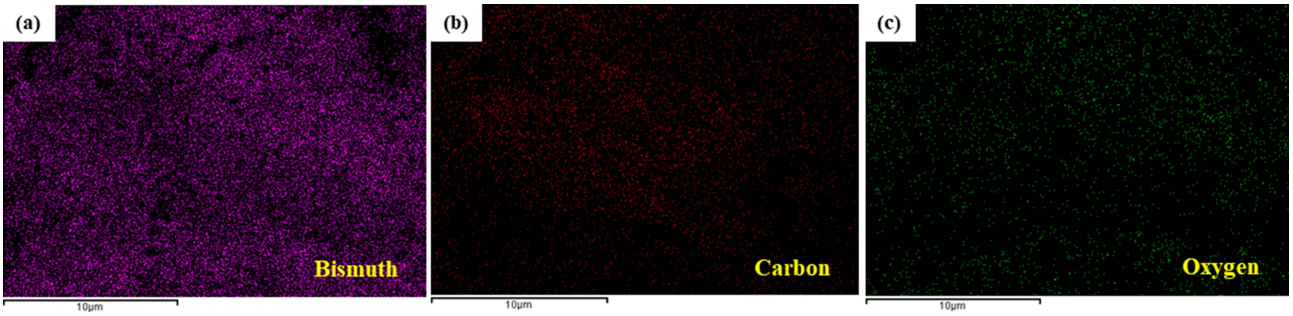

Figure 3 Elemental mapping of Bi_2O_3/RGO nanocomposites. (**a**) bismuth, (**b**) carbon, and (**c**) oxygen mapping.

elemental composition, as determined by EDS, is presented in Figure 5. The EDS spectra approve the occurrence of Bi, O, and C elements with no contaminations. The manifestation of Cu peak was a result of the employment of a TEM grid made from copper metal.

XPS Study

The XPS technique was utilized to analyze the composition and chemical states of the Bi_2O_3/RGO nanocomposite. Based on the data presented in Figure 6a, it is evident that there are two distinct peaks at binding energies of 161.04 and 166.34

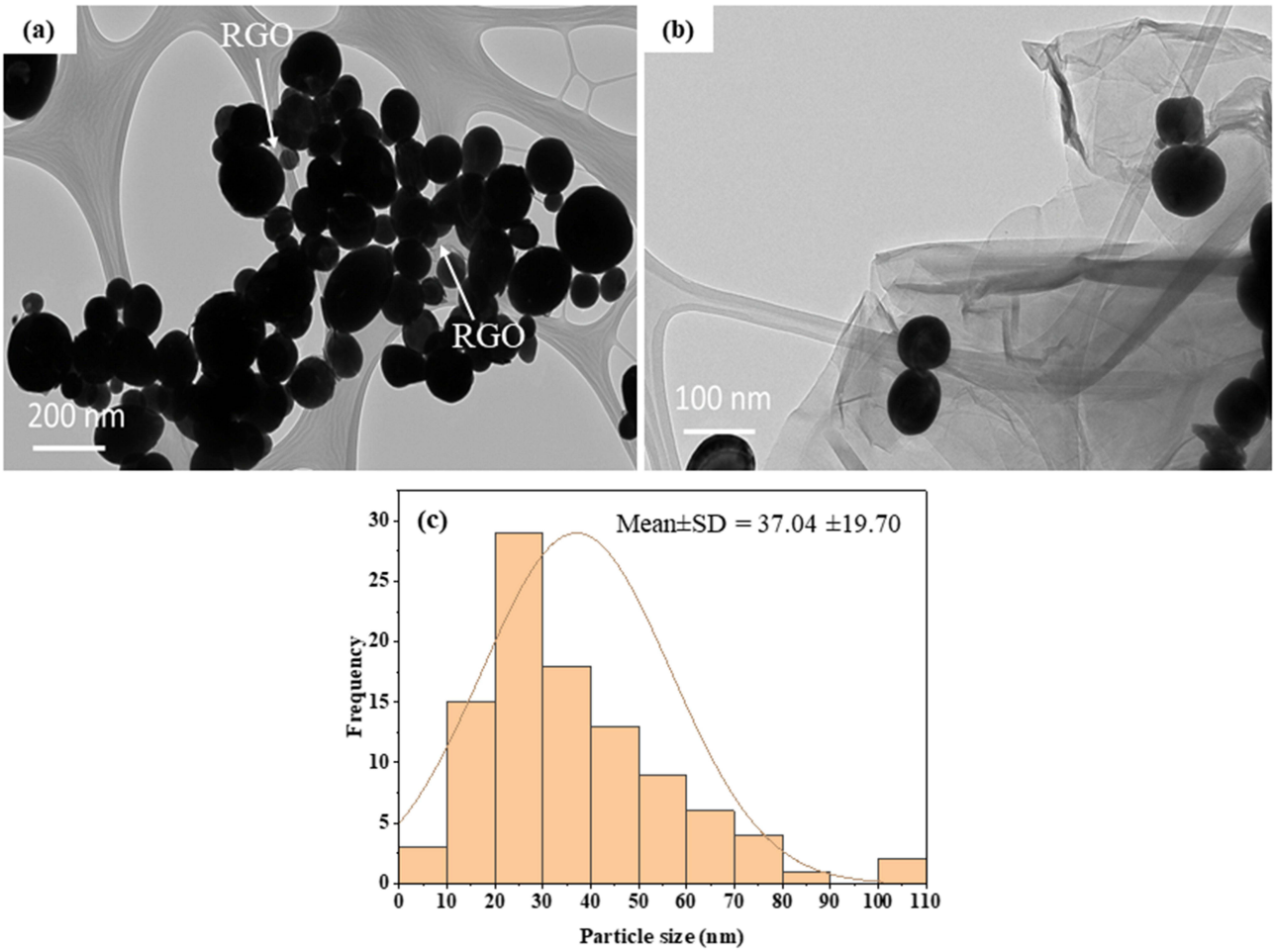

Figure 4 TEM characterization of Bi_2O_3/RGO nanocomposites. (**a** and **b**) TEM micrographs, and (**c**) particle size distribution.

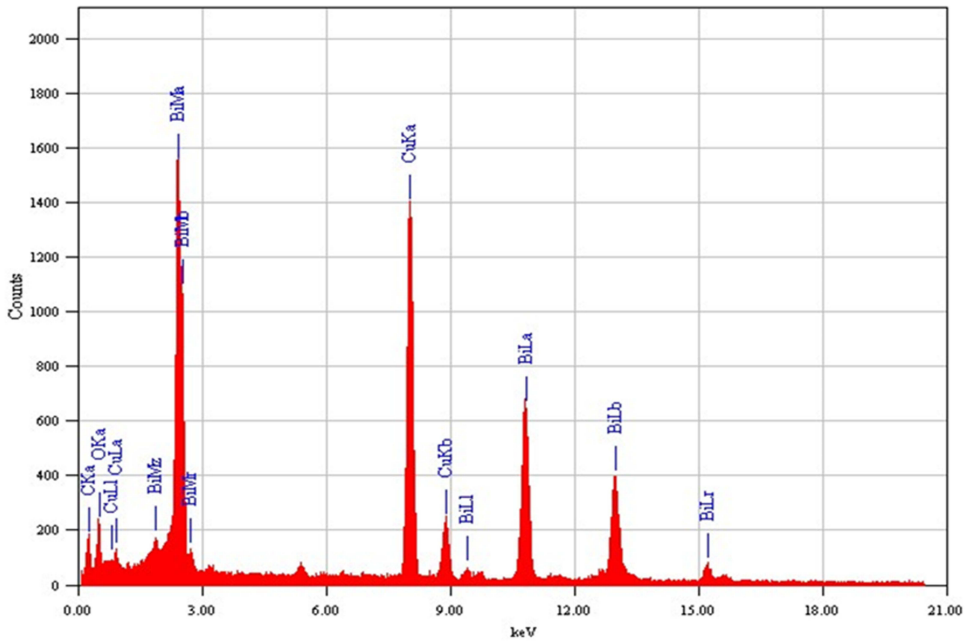

Figure 5 Elemental composition of Bi_2O_3/RGO nanocomposites analyzed by EDS associated with TEM.

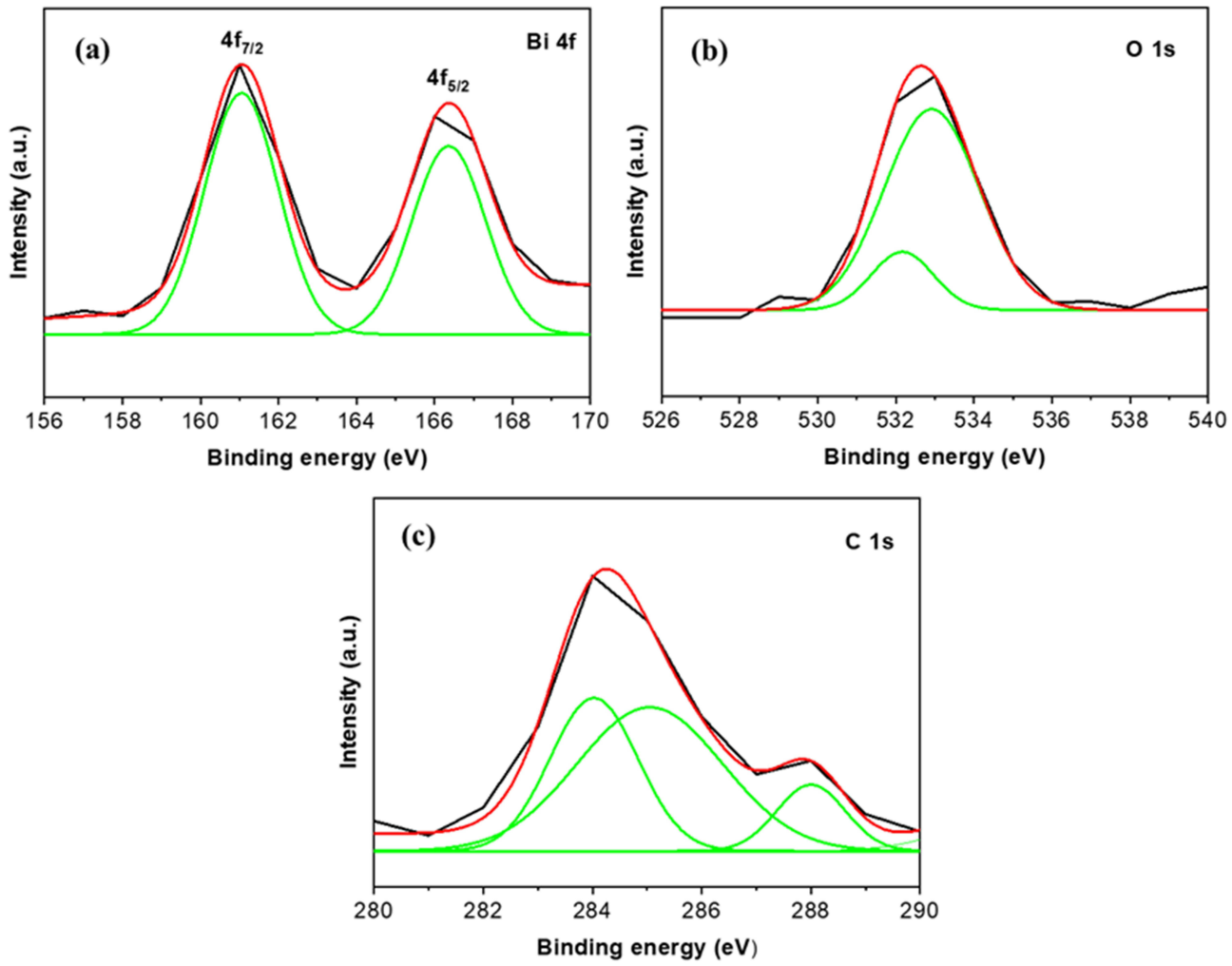

Figure 6 XPS spectra of Bi_2O_3/RGO nanocomposites. (**a**) Bi 4f, (**b**) O 1s, and (**c**) C 1s.

eV. These peaks can be attributed to the presence of Bi 4f7/2 and 4f5/2, respectively. This observation strongly suggests that the material contains Bi in its +3 oxidation state. In Figure 6b, the O 1s spectrum showed two peaks at binding energies located at 532.19 and 532.92 eV. These were caused by metal oxygen bonding from Bi_2O_3. Figure 6c shows C1s spectra of Bi_2O_3/RGO nanocomposite showed three clear peaks at 284.03, 285.09, and 288.05 eV, which correspond to the C-C, C=O, and O-C=O groups, respectively, and provide evidence for the existence of RGO. The current XPS measurements of Bi_2O_3/RGO nanocomposites are consistent with the findings of prior research.[34–36]

DLS Study

Evaluating the behavior of nanoscale materials in biological environments is crucial for comprehending the interaction between nanostructures and biological systems.[18] The colloidal properties of the Bi_2O_3/RGO nanocomposites in the culture medium (DMEM without supplements) were further examined using the DLS. The distribution of hydrodynamic size of Bi_2O_3/RGO nanocomposites in the culture medium was calculated to be 167 nm (Figure 7a), which is approximately 4–5 folds larger as compared to the particle size computed from TEM, SEM, and XRD in the powder form. The increased hydrodynamic size may be attributed to the aggregation of particles in a water-based suspension, as documented in earlier research.[56,57] The propensity of particles to aggregate is contingent upon the surface charge. The zeta potential study discovered that particles possessed a surface charge of around −10 eV in the cell culture medium (Figure 7b). The negative value of the zeta potential suggests the occurrence of negatively charged functional groups on

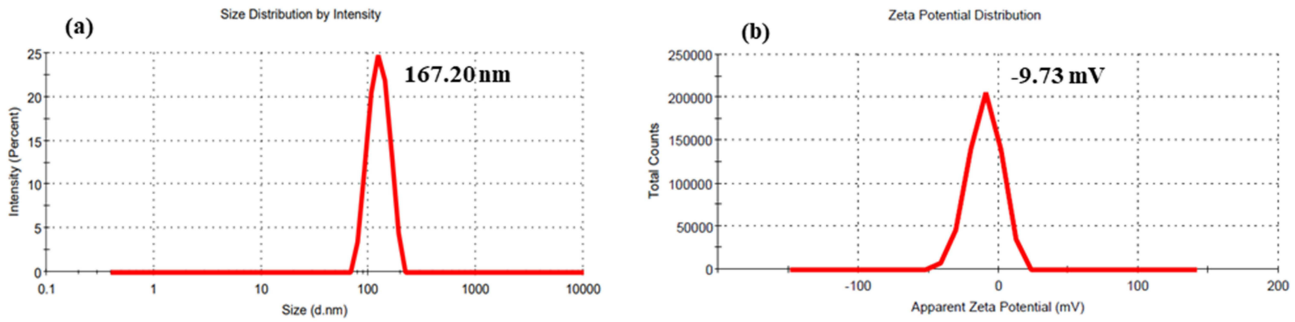

Figure 7 DLS characterization of Bi_2O_3/RGO nanocomposites in cell culture medium. (**a**) hydrodynamic size and (**b**) zeta potential.

the surface of nanocomposite. These results indicate that the colloidal suspension of the current nanocomposites in a physiological medium exhibited a good level of stability. The physicochemical characterization of Bi_2O_3/RGO nanocomposites is summarized in Table 1. This finding aligns well with previous research.[58,59] For instance, a recently synthesized Bi_2O_3-RGO nanocomposite synthesized through hydrothermal route by implementing green reduction of GO exhibited almost similar physicochemical characteristics with the Bi_2O_3/RGO nanocomposite explored in this study.[58]

Cytotoxicity Study

The harmful effects of Bi_2O_3 nanoparticles and their nanocomposite forms have been identified as a significant constraint for their widespread uses, thus necessitating a thorough toxicological assessment of such nanostructured materials.[5] The small size and unique physiochemical features of nanoscale materials may give rise to undesirable effects.[6] This work investigated the cytotoxicity of Bi_2O_3/RGO nanocomposites in two distinct mammalian cell lines- NRK52E and HepG2. Bi_2O_3/RGO nanocomposites were added to both cell types with a range of concentrations (from 1 to 400 µg/mL) for various time-intervals (24–72 h). The cytotoxicity of nanocomposites was assessed using the MTT test. This experiment is a highly sensitive and frequently employed assay to assess the cytotoxicity of drugs, chemicals, and nanoscale materials at the in vitro level.[16,17] The results of these experiments revealed that Bi_2O_3/RGO nanocomposites exhibit cytotoxic effects on both NRK52E and HepG2 cells, with the level of cytotoxicity relying on the dosage and time of exposure (Figures 8a and 8b). The half maximum inhibitory concentrations (IC_{50}) of Bi_2O_3/RGO nanocomposites in NRK52E cells were 98, 25, and 9 µg/mL after 24, 48, and 72 h, respectively. In addition, the IC_{50} values of Bi_2O_3/RGO nanocomposites in HepG2 cells were 88, 70, and 53 µg/mL for 24, 48, and 72 h, respectively (Table 2). Previous research

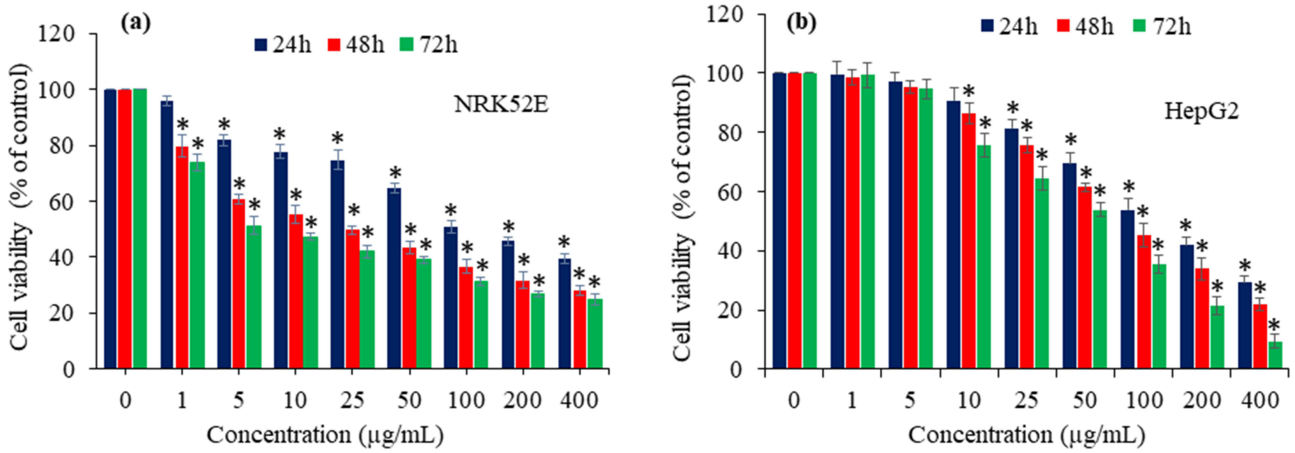

Figure 8 Cytotoxic effect of Bi_2O_3/RGO nanocomposites in two distinct mammalian cell lines. (**a**) dose- and time-dependent cytotoxicity in NRK52E cells and (**b**) dose- and time-dependent cytotoxicity in HepG2 cells. Data are represented as the mean±SD of three separate experiments (n = 3). *Significantly different as compared to the control ($p<0.05$).

Table 2 The IC_{50} Values of Bi_2O_3/RGO Nanocomposites in Two Distinct Mammalian Cell Lines for Different Exposure Times. The IC_{50} Values Were Calculated Using GraphPad Software

Exposure Time	NRK52E cells	HepG2 cells
24 h	98.43 µg/mL	88.24 µg/mL
48 h	24.79 µg/mL	70.08 µg/mL
72 h	9.39 µg/mL	53.42 µg/mL

has also revealed the harmful impact of Bi_2O_3 nanoparticles and nanocomposites in biological systems. Liman (2013) documented that Bi_2O_3 had genotoxic effects on the root cells of *Allium cepa*.[19] Negative impact of Bi_2O_3 nanoparticles on the eggs of zebra fish is also reported.[20] A recent study found that rGO-Bi_2O_3 nanocomposites exert cytotoxic effects in A549 and NCI-H460 lung cancer cells.[58]

Interestingly, NRK52E cells exhibit slightly greater vulnerability to Bi_2O_3/RGO nanocomposites compared to HepG2 cells. Similar to this work, earlier we observed that human fibrosarcoma epithelial cells (HT1080) were more susceptible to MnO_2 nanostructures than those of human breast cancer cells (MCF-7). This was due to the higher level of MnO_2 uptake by HT1080 cells compared to MCF-7 cells.[5] In this study, however, the cellular uptake study for Bi_2O_3/RGO nanocomposites in both the NRK52E and HepG2 cells was not examined. Moreover, this research paves the way for future in-depth investigations aimed at exploring the potential mechanisms of varying sensitivity of different cell types against Bi_2O_3/RGO nanocomposites.

Intracellular ROS Generation

Researchers have proposed that ROS-induced oxidative stress is the probable mechanism of toxicity generated by nanostructured materials.[60,61] ROS might function as a signalling species to induce many cellular processes, including apoptosis and genotoxicity.[62] ROS generated oxidative stress has been found to be linked to various human disorders such as diabetes, neurodegeneration, cancer, and heart disease.[63] Here, we assessed the impact of Bi_2O_3/RGO nanocomposites on the intracellular creation of ROS in NRK52E and HepG2 cell lines. Both types of cells were subjected to Bi_2O_3/RGO nanocomposites exposure at concentrations of 10–200 µg/mL for a duration of 48 h. The findings demonstrated that the Bi_2O_3/RGO nanocomposites caused the production of ROS in both cell types, with the level of ROS formation being dependent on the concentration of the nanocomposites ($p < 0.05$) (Figure 9a and b). Moreover, images taken with a fluorescent microscope showed that the DCF probe (a biomarker of ROS production) fluoresced much brighter in cells (NRK52E and HepG2) treated with Bi_2O_3/RGO nanocomposites than the control groups (Figure 9c). In previous investigation, we showed that pure Bi_2O_3 nanoparticles induce ROS generation in HUVE cells and mouse spermatogonia cells.[64,65] The present results are also supported by multiple earlier studies that show different metal oxide nanoparticles (eg ZnO, NiO, and CuO) increase the level of ROS in cells.[66–68] Moreover, our recent work found that CuO/RGO nanocomposites induce intracellular ROS level in NRK52E cells.[42]

The structure and composition of Bi_2O_3/RGO nanocomposites could play a key role in ROS generation in selected NRK52E and HepG2 cells. The high surface area, surface oxygen functional groups, and crystalline nature of nanocomposites could all contribute to intracellular ROS generation.[65–67] However, these results warrant further research to establish correlations between the physicochemical properties of Bi_2O_3/RGO nanocomposites and intracellular ROS production.

Intracellular Glutathione Depletion

The equilibrium between the production of pro-oxidants, such as ROS, and their counteraction by antioxidants, such as GSH, is highly sensitive. Oxidative detriment to cell biomolecules (eg DNA, lipids, and proteins) occurs when there is an excessive synthesis of pro-oxidants or a decrease in antioxidants.[69] GSH is a naturally occurring tripeptide that is essential for

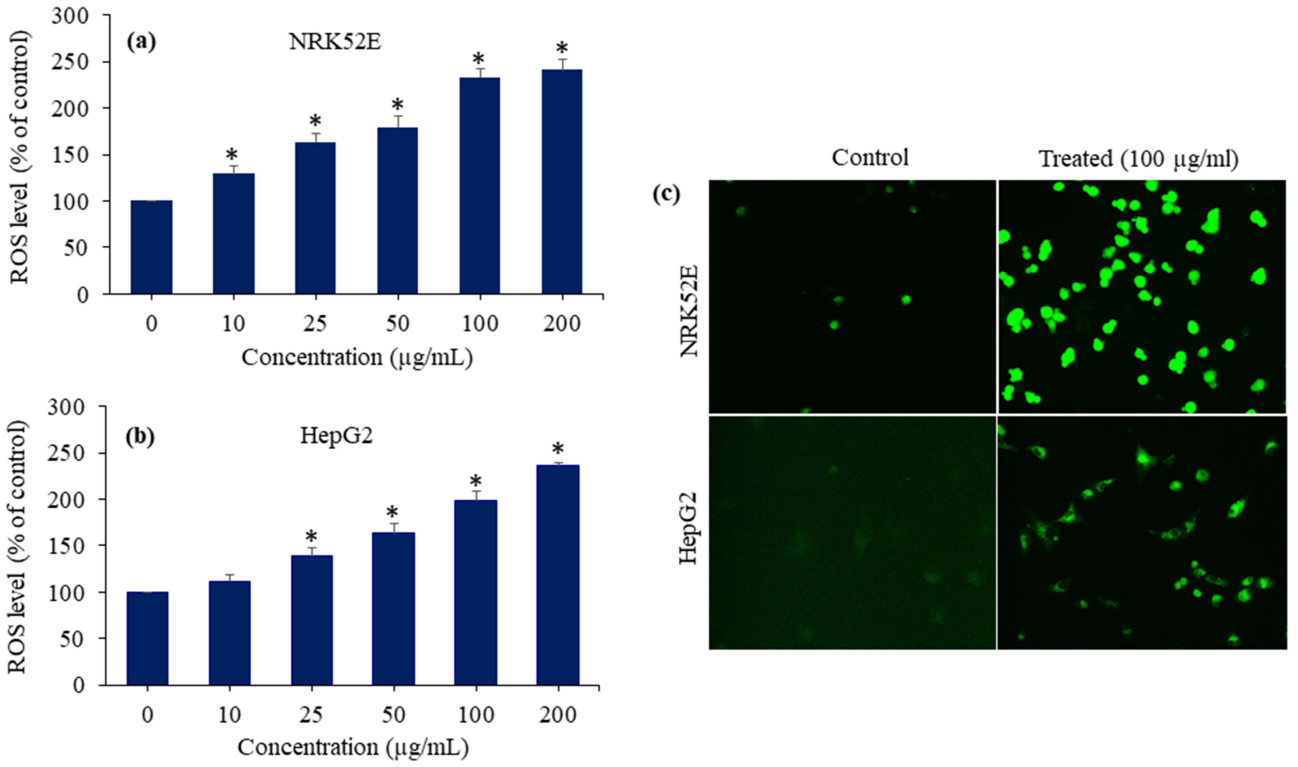

Figure 9 ROS-generating potential of Bi_2O_3/RGO nanocomposites in two distinct mammalian cell lines. (**a**) ROS generation in NRK52E cells exposed to Bi_2O_3/RGO nanocomposites for 48 h. (**b**) ROS generation in HepG2 cells exposed to Bi_2O_3/RGO nanocomposites for 48 h. (**c**) Fluorescent microscopy images of ROS generation in NRK52E and HepG2 cells after exposure to 100 µg/mL of Bi_2O_3/RGO nanocomposites for 48 h. Quantitative data is represented as the mean±SD of three separate experiments (n=3). *Significantly different as compared to the control ($p<0.05$).

maintaining the equilibrium of cellular redox through its antioxidant properties. GSH is also discovered to be coupled with the instigation of apoptosis.[70] A comprehensive understanding of the fundamental mechanisms behind the toxicity of nanocomposites has yet to be fully elucidated. Here, we inspected the impact of Bi_2O_3/RGO nanocomposites in GSH contents of NRK52E and HepG2 cell lines. Both cell types were exposed to 10, 25, 50, 100, and 200 µg/mL concentrations of nanocomposites for a duration of 48 h. Results showed that the level of GSH in both types of cells (NRK52E and HepG2) depleted with increasing the concentration of Bi_2O_3/RGO nanocomposites (Figures 10a and 10b). The findings suggest that the Bi_2O_3/RGO nanocomposites cause cytotoxicity in mammalian cells by disrupting the balance of redox reactions.

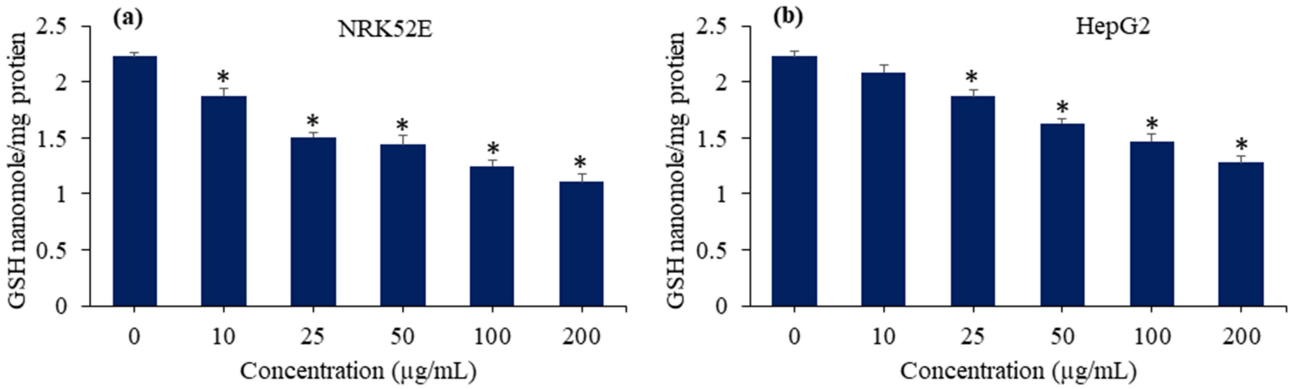

Figure 10 GSH-depleting potential of Bi_2O_3/RGO nanocomposites in two distinct mammalian cell lines. (**a**) GSH depletion in NRK52E cells exposed to Bi_2O_3/RGO nanocomposites for 48 h. (**b**) GSH depletion in HepG2 cells exposed to Bi_2O_3/RGO nanocomposites for 48 h. Data are represented as the mean±SD of three separate experiments (n=3). *Significantly different as compared to the control ($p<0.05$).

Caspase-3 Enzyme Activation and Chromosomal Condensation

Apoptosis activates caspases in many cells, and they play a key role in initiating and completing apoptosis.[17] Caspase-3 gene plays crucial role in DNA damage and apoptotic process.[71] In this work, we examined the enzymatic function of the caspase-3 enzyme to understand the possible impact of Bi_2O_3/RGO nanocomposites on apoptosis. NRK52E and HepG2 cell lines were treated at different concentrations (10 to 200 µg/mL) of Bi_2O_3/RGO nanocomposites for a duration of 48 h. Figure 11a and b, clearly showed that the enzymatic activity of caspase-3 in both cell types increases concentration-dependently after being exposed to Bi_2O_3/RGO nanocomposites.

The assessment of cell shrinkage and chromatin condensation is fundamental for the morphological analysis of apoptotic cell death.[72] DAPI is a fluorophore that specifically binds to nucleic acids and is commonly employed for labelling chromosomes.[73] Due to the weakened apoptotic cell membrane, an increased amount of DAPI enters the cell, resulting in a more intense blue stain. The distinct nuclear characteristics shown by apoptotic cells, such as chromosomal condensation and fragmentation, aid in the visual detection of apoptotic cells that have been stained with DAPI.[74] Ali and colleagues[75] observed the process of chromosomal condensation in HepG2 cells after exposure to rGO-Ag nanocomposites using Hoechst 33342 labelling. This study also investigated chromosomal condensation using DAPI labelling in NRK52E and HepG2 after being exposed to 100 µg/mL of Bi_2O_3/RGO nanocomposites for a duration of 48 h. Fluorescent images of DAPI revealed that Bi_2O_3/RGO nanocomposites effectually induce condensation of chromosomes in both cell types (Figure 11c).

Detection of Apoptotic Cells by Acridine Orange-Ethidium Bromide (AO-EB) Dual Fluorescent Probe

AO-EB dual staining is a qualitative method that utilizes fluorescence images to detect nuclear alterations and apoptotic body formation in cells. This technique is effective to identify live, necrotic, and apoptotic cells.[76] AO is a fluorescent dye that specifically binds to nucleic acids. This substance exhibits cell permeability and has the ability to stain both live and dead cells. However, EB can only enter the damaged membrane of late apoptotic and necrotic cells, where it emits a bright orange or red fluorescence as it binds to DNA fragments or the apoptotic moiety in these cells. Apoptotic cells

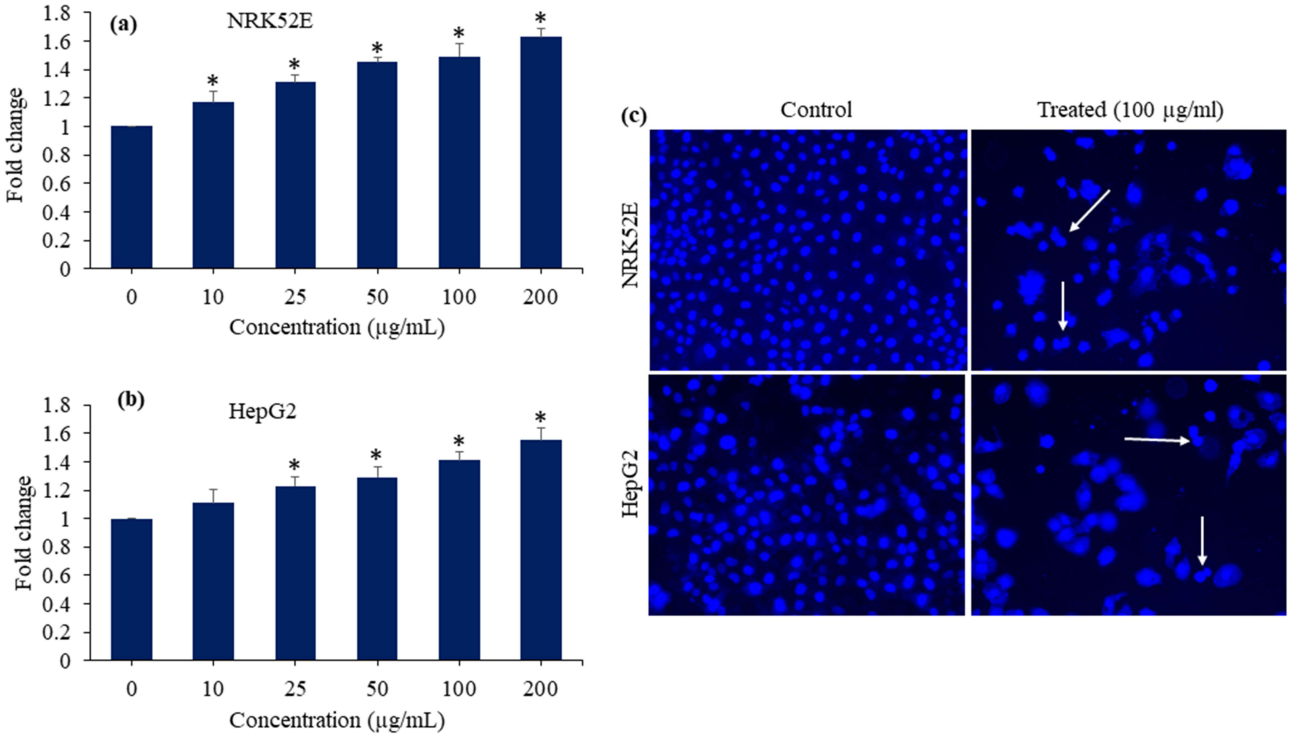

Figure 11 Caspase-3 enzyme activation and chromosomal condensation of Bi_2O_3/RGO nanocomposites in two distinct mammalian cell lines. (**a**) and (**b**) Caspase-3 enzyme activity in NRK52E and HepG2 cells exposed to Bi_2O_3/RGO nanocomposites for 48 h. (**c**) Fluorescent microscopy images of chromosomal condensation by DAPI staining NRK52E and HepG2 cells after exposure to 100 µg/mL of Bi_2O_3/RGO nanocomposites for 48 h. Quantitative data is represented as the mean±SD of three separate experiments (n=3). *Significantly different as compared to the control ($p<0.05$). White arrows indicate the condensation of chromosomes.

display compacted chromatin and exhibit an orange-red color (AO-EB staining) in contrast to the healthy cells, which look green (AO staining only) when detected by a fluorescent microscope.[77] In this work, the apoptotic consequences of Bi_2O_3/RGO nanocomposites in NRK52E and HepG2 cell lines were evaluated by employing AO-EB dual labelling. Figure 12a demonstrates that the control cells had a consistent green color, indicating the presence of viable and healthy

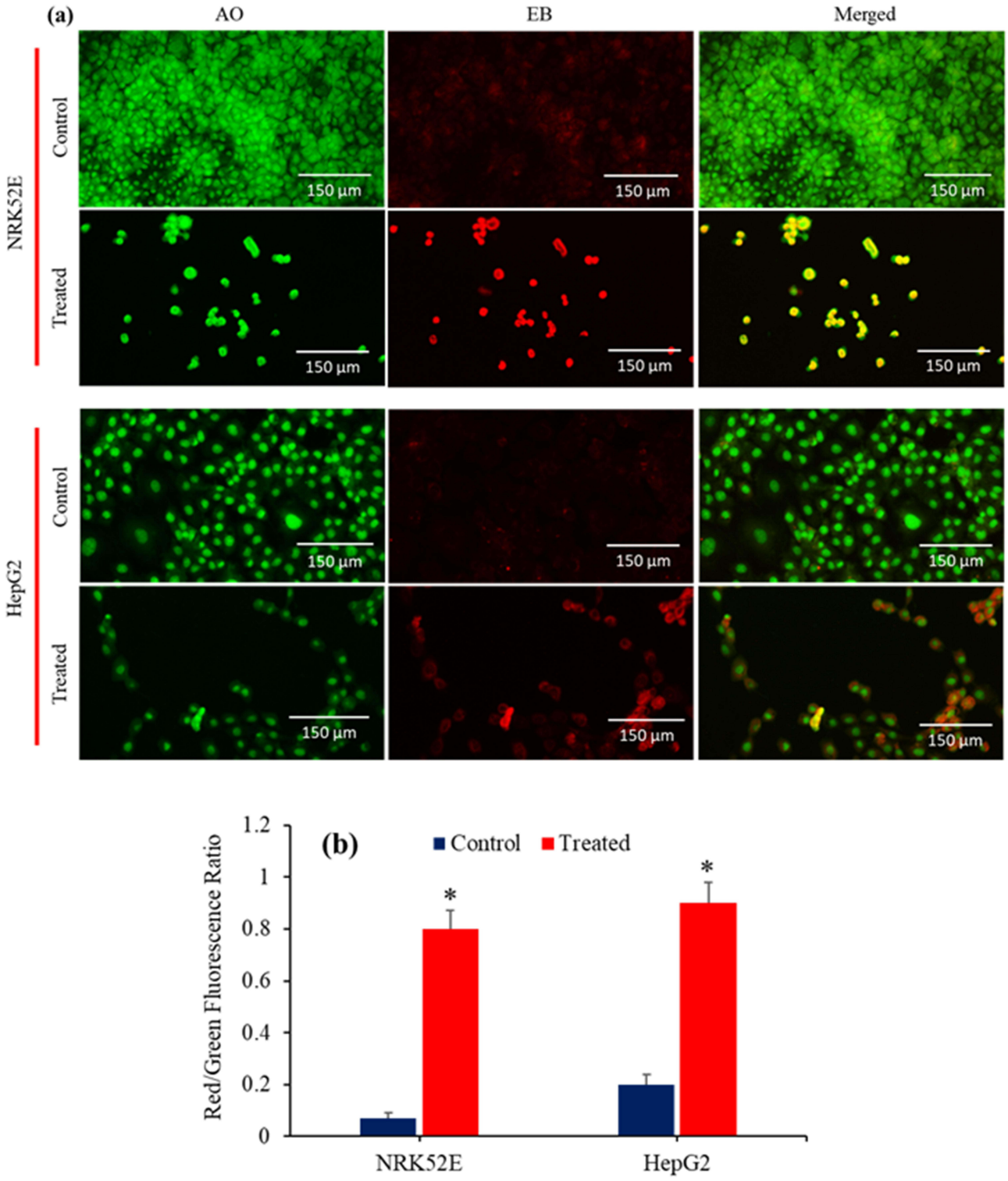

Figure 12 (**a**) AO-EB dual staining to study the apoptosis response in NRK52E and HepG2 cells following exposure to Bi_2O_3/RGO nanocomposites for 48 h. Apoptosis cells emit an Orange-red fluorescence stain, whereas healthy cells emit green fluorescence. (**b**) Graphical representation of red/green fluorescence ratio. Quantitative data is represented as the mean±SD of three separate experiments (n=3). *Significantly different as compared to the control ($p<0.05$).

cells. Exposure to Bi_2O_3/RGO nanocomposites resulted in the emergence of orange-red nuclei in many cell populations in both types of cells. The changing proportion of green to red fluorescence indicated that the control cells were in a healthy state, whereas the exposed cells were likely undergoing apoptosis (Figure 12b). The results clearly found that the AO/EB staining method effectively differentiates between normal cells and apoptotic cells, providing evidence of apoptosis induction by Bi_2O_3/RGO nanocomposites in both NRK52E and HepG2 cells. In a previous study, it was demonstrated that NRK52 cells treated with CuO nanoparticles decorated on RGO sheets displayed a notable increase in apoptotic cells, as determined by the AO-EB dual staining technique.[42]

Flow Cytometry Analysis of Cell Cycle

Exploration of the cell cycle is an important factor for a comprehensive understanding of the toxicity generated by nanoscale materials.[78] Multiple reports have demonstrated that metal oxide nanoparticles and graphene derivatives cause toxicity in biological systems by disturbing the progression of cell cycle.[42,79] A recent study perceived that α-Fe_2O_3-sodium alginate-thymoquinone nanocomposites have a damaging effect on breast cancer MDA-MB-231 cells by inducing higher levels of oxidative stress, promoting apoptosis, and causing cell cycle interruption.[80] High ROS levels in NRK52E and HepG2 cells treated with Bi_2O_3/RGO nanocomposites suggest the potential for DNA damage and apoptosis. This effect is noticeable in the early stages of cell cycle development. Genetically damaged cells congregate in G1, S, or G2/M phases of the cell cycle.[79] Cells that have incurred irreversible damage undergo apoptosis, a process that

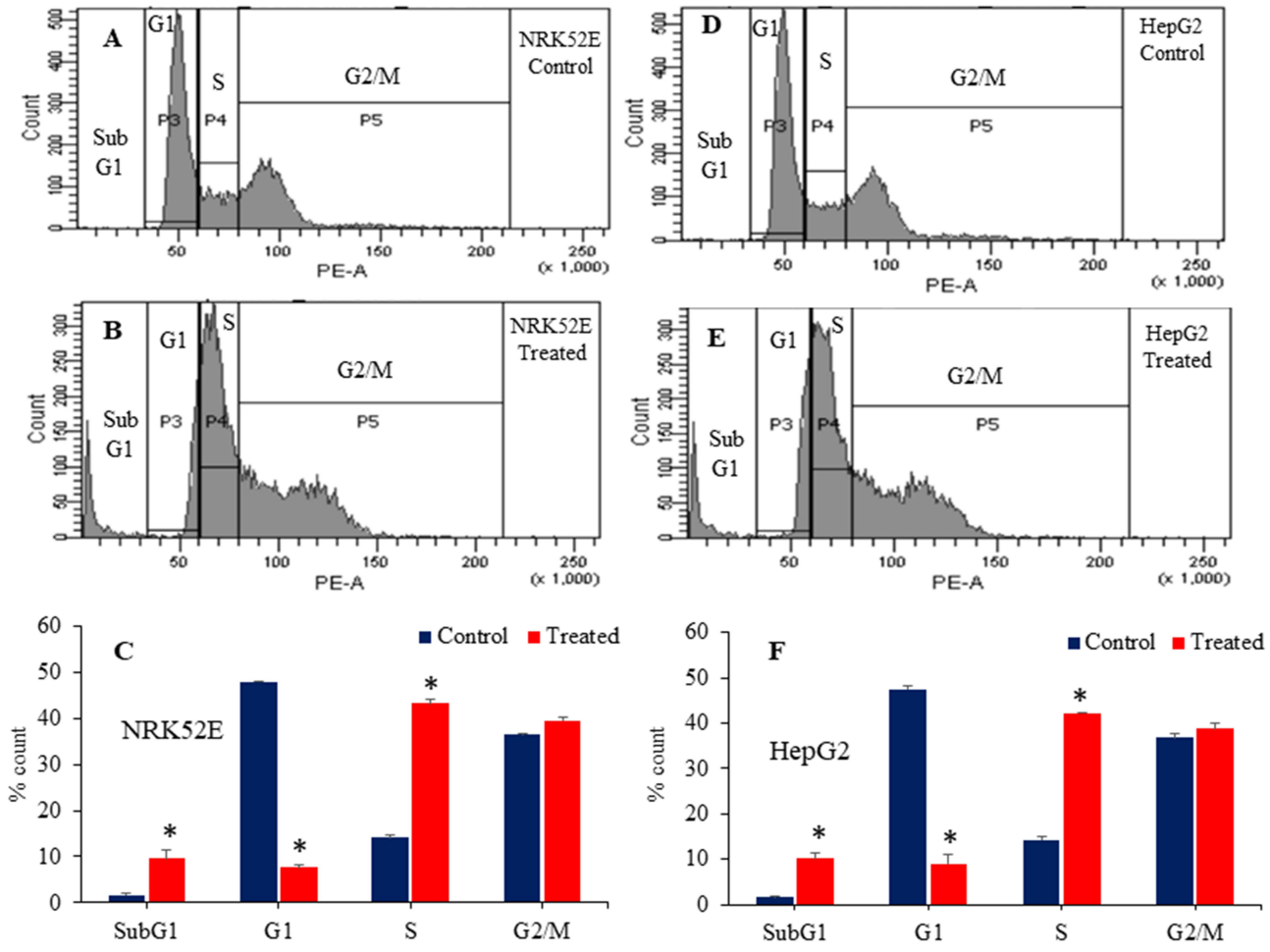

Figure 13 Cell cycle analysis of NRK52E and HepG2 cells following exposure to 100 µg/mL of Bi_2O_3/RGO nanocomposites for 48 h. Histogram of control (**A**), treated (**B**), and the percentage of cell population in subG1, G1, S, and G2/M phases (**C**) of NRK52E cells. Histogram of control (**D**), treated (**E**), and the percentage of cell population in subG1, G1, S, and G2/M phases (**F**) of HepG2 cells. Quantitative data is represented as the mean±SD of three separate experiments (n=3). *Significantly different as compared to the control ($p<0.05$).

leads to an increase in cells in the sub-G1 phase. This work further investigated the toxicological examination of Bi_2O_3/RGO nanocomposites in NRK52E and HepG2 cells through cell cycle analysis. Flow cytometry examination of the cell cycle demonstrated the initiation of apoptosis in NRK52E and HepG2 cell lines following exposure of Bi_2O_3/RGO nanocomposites (100 µg/mL for 48 h). Results showed that the Bi_2O_3/RGO nanocomposites-treated NRK52E cells exhibited a higher percentage (9.7%) of cells in subG1 than the control group (2%) (Figure 13A–C). In HepG2 cells, there was a 10.2% increase in cell number in treated group compared to control group, which only had a 1.5% accumulation (Figure 13D–F). Furthermore, the impact of Bi_2O_3/RGO nanocomposites on cell cycle arrest in both cell types was also evident by alterations in G1 and S phases.

To mitigate the detrimental impacts of metal oxide-based nanocomposites without compromising their beneficial biological properties, investigators are exploring a number of different strategies. Integrating Bi_2O_3-based nanostructures with other therapeutic substances could be one of the possible tactics. Nevertheless, it is crucial to perform a comprehensive toxicity study of any newly developed therapeutic agents prior to their biomedical applications.

Conclusion

Two distinct mammalian cell lines, NRK52E and HepG2, were used to examine the hazardous potential of Bi_2O_3/RGO nanocomposites. TEM, SEM, XRD, EDS, and DLS studies validated the preparation of high quality of Bi_2O_3/RGO nanocomposites. The biological findings showed that the Bi_2O_3/RGO nanocomposites cause cytotoxicity in both NRK52E and HepG2 cells in a time- and concentration-dependent mode. Importantly, NRK52E exhibited greater susceptibility to Bi_2O_3/RGO nanocomposites compared to HepG2 cells. Bi_2O_3/RGO nanocomposites were observed to produce oxidative stress by generating pro-oxidant ROS and depleting the antioxidant GSH in both cell types. The exposure to Bi_2O_3/RGO nanocomposites resulted in the activation of the Caspase-3 enzyme and chromosomal condensation in both NRK52E and HepG2 cells. AO-EB dual staining and cell cycle analysis data indicated the apoptosis response of Bi_2O_3/RGO nanocomposites. Altogether, these results suggest that the toxicity of Bi_2O_3/RGO nanocomposites in both NRK52E and HepG2 cells is caused by its ability to induce the ROS generation, resulting in cell cycle disturbance and apoptosis. These results suggest the adverse effects of biomedically relevant Bi_2O_3-based nanocomposites on human health. This study paves the way for future work to outline the probable toxicity mechanisms of Bi_2O_3/RGO nanocomposites in animal systems.

Acknowledgment

The authors acknowledge the Research Institute/Centre supporting program (RICSP-24-1), King Saud University, Riyadh, Saudi Arabia.

Author`s Contribution

All authors made substantial contributions to conception and design, acquisition of data, or analysis and interpretation of data; took part in drafting the article or revising it critically for important intellectual content; agreed to submit to the current journal; gave final approval of the version to be published; and agreed to be accountable for all aspects of the work.

Disclosure

The authors report no conflicts of interest in this work.

References

1. Malik S, Muhammad K, Waheed Y. Nanotechnology: a revolution in modern industry. *Molecules*. 2023;28(2):661. doi:10.3390/molecules28020661
2. Saritha GNG, Anju T, Kumar A. Nanotechnology—Big impact: how nanotechnology is changing the future of agriculture? *J Agric Food Res*. 2022;10:100457. doi:10.1016/j.jafr.2022.100457
3. Ahamed M, Akhtar MJ, Alhadlaq HA, Alrokayan SA. Assessment of the lung toxicity of copper oxide nanoparticles: current status. *Nanomedicine*. 2015;10(15):2365–2377. doi:10.2217/nnm.15.72
4. Joudeh N, Linke D. Nanoparticle classification, physicochemical properties, characterization, and applications: a comprehensive review for biologists. *J Control Release*. 2022;20(1):262. doi:10.1186/s12951-022-01477-8

5. Alhadlaq HA, Akhtar MJ, Ahamd M. Different cytotoxic and apoptotic responses of MCF-7 and HT1080 cells to MnO_2 nanoparticles are based on similar mode of action. *Toxicology*. 2019;411:71–80. doi:10.1016/j.tox.2018.10.023
6. Xuan L, Ju Z, Skonieczna M, Zhou PK, Huang R. Nanoparticles-induced potential toxicity on human health: applications, toxicity mechanisms, and evaluation models. *Med Comm*. 2023;4(4):e327. doi:10.1002/mco2.327
7. Ahamed M, Akhtar MJ, Khan MM, Alhadlaq HA. Improved antimicrobial and anticancer potential of eco-friendly synthesized Co-doped Bi2O3/RGO nanocomposites. *J Drug Deliv Sci Technol*. 2023;84:104525. doi:10.1016/j.jddst.2023.104525
8. Shahbazi MA, Faghfouri L, Ferreira MP, et al. The versatile biomedical applications of bismuth-based nanoparticles and composites: therapeutic, diagnostic, biosensing, and regenerative properties. *Chem Soc Rev*. 2020;125:3–21. doi:10.1039/C9CS00283A
9. Zulkifli ZA, Razak KA, Rahman WN, Abidin SZ. Synthesis and characterisation of bismuth oxide nanoparticles using hydrothermal method: the effect of reactant concentrations and application in radiotherapy. *J Phys*. 2018;1082:012103.
10. Bogusz K, Tehei M, Stewart C, et al. Synthesis of potential theranostic system consisting of methotrexate-immobilized (3-aminopropyl) trimethoxysilane coated α-Bi2O3 nanoparticles for cancer treatment. *RSC Adv*. 2014;4:24412–24419. doi:10.1039/C4RA02160F
11. Abidin SZ, Razak KA, Zin H, et al. Comparison of clonogenic and PrestoBlue assay for radiobiological assessment of radiosensitization effects by bismuth oxide nanorods. *Today Proc*. 2019;16:1646–1653. doi:10.1016/j.matpr.2019.06.030
12. Zainudin NH, Ab Razak K, Abidin SZ, Abdullah R, Rahman WN. Influence of bismuth oxide nanoparticles on bystander effects in MCF-7 and hFOB 1.19 cells under 10 MV photon beam irradiation. *Radiat Phys Chem*. 2020;177:109143. doi:10.1016/j.radphyschem.2020.109143
13. Hernandez-Delgadillo R, Velasco-Arias D, Martinez-Sanmiguel JJ, et al. Bismuth oxide aqueous colloidal nanoparticles inhibit Candida albicans growth and biofilm formation. *Int J Nanomed*. 2013;24:1645–1652. doi:10.2147/IJN.S38708
14. Geoffrion LD, Medina-Cruz D, Kusper M, et al. Bi_2O_3 nano-flakes as a cost-effective antibacterial agent. *Nanoscale Adv*. 2021;4:4106–4118. doi:10.1039/D0NA00910E
15. Karthik R, Pandiselvi K, Mariyappan K, Park K, Kwak IS, Sivakamavalli J. Synthesis of biogenic chitosan biopolymer-functionalized zinc-doped Bi2O3 nanoneedles and its bio-applications: in vitro antibacterial and anticancer activity. *Arab J Sci Eng*. 2021;46:5605–5618. doi:10.1007/s13369-020-05099-w
16. Abudayyak M, Öztaş E, Arici M, Özhan G. Investigation of the toxicity of bismuth oxide nanoparticles in various cell lines. *Chemosphere*. 2017;169:117–123. doi:10.1016/j.chemosphere.2016.11.018
17. Ahamed M, Akhtar MJ, Khan MM, Alrokayan SA, Alhadlaq HA. Oxidative stress mediated cytotoxicity and apoptosis response of bismuth oxide (Bi_2O_3) nanoparticles in human breast cancer (MCF-7) cells. *Chemosphere*. 2019;216:823–831. doi:10.1016/j.chemosphere.2018.10.214
18. Ahamed M, Akhtar MJ, Khan MM, Alaizeri ZM, Alhadlaq HA. Facile synthesis of Zn-doped Bi2O3 nanoparticles and their selective cytotoxicity toward cancer cells. *ACS Omega*. 2021;17:353–356. doi:10.1021/acsomega.1c01467
19. Liman R. Genotoxic effects of Bismuth (III) oxide nanoparticles by allium and comet assay. *Chemosphere*. 2013;93(2):269–273. doi:10.1016/j.chemosphere.2013.04.076
20. Kovrižnych JA, Sotníková R, Zeljenková D, Rollerová E, Szabová E, Wimmerová S. Acute toxicity of 31 different nanoparticles to zebrafish (*Danio rerio*) tested in adulthood and in early life stages–comparative study. *Interdiscip Toxicol*. 2013;6(2):67–73. doi:10.2478/intox-2013-0012
21. Reiss T, Hjelt K, Ferrari AC. Graphene is on track to deliver on its promises. *Nat Nanotechnol*. 2019;14:907–910. doi:10.1038/s41565-019-0557-0
22. Li M, Yin B, Gao C, Guo J, Zhao C, Guo X. Graphene: preparation, tailoring, and modification. *Exploration*. 2023;3(1):20210233. doi:10.1002/EXP.20210233
23. Lalwani G, D'Agati M, Khan AM, Sitharaman B. Toxicology of graphene-based nanomaterials. *Adv Drug Deliv Rev*. 2016;105:109–144. doi:10.1016/j.addr.2016.04.028
24. Martín C, Kostarelos K, Prato M, Bianco A. Biocompatibility and biodegradability of 2D materials: graphene and beyond. *Chem Comm*. 2019;55:5540–5546. doi:10.1039/C9CC01205B
25. Kumar S, Kaushik RD, Purohit LP. Novel ZnO tetrapod-reduced graphene oxide nanocomposites for enhanced photocatalytic degradation of phenolic compounds and MB dye. *J Mol Liq*. 2021;327:114814. doi:10.1016/j.molliq.2020.114814
26. McCallion C, Burthem J, Rees-Unwin K, Golovanov A, Pluen A. Graphene in therapeutics delivery: problems, solutions and future opportunities. *Eur J Pharm Biopharm*. 2016;104:235–250. doi:10.1016/j.flatc.2022.100417
27. Chiticaru EA, Ionita M. Graphene toxicity and future perspectives in healthcare and biomedicine. *FlatChem*. 2022;35:100417. doi:10.1016/j.flatc.2022.100417
28. Lazăr AI, Aghasoleimani K, Semertsidou A, et al. Graphene-related nanomaterials for biomedical applications. *Nanomaterials*. 2023; 13(6):1092. doi:10.3390/nano13061092
29. Shareena Dasari TP, McShan D, Dasmahapatra AK, Tchounwou PB. A review on graphene-based nanomaterials in biomedical applications and risks in environment and health. *Nano-Micro Lett*. 2018;10:1–34. doi:10.1007/s40820-018-0206-4
30. Volkov Y, McIntyre J, Prina-Mello A, Graphene toxicity as a double-edged sword of risks and exploitable opportunities: a critical analysis of the most recent trends and developments. *2D Mater*. 2017;4(2):022001. doi:10.1088/2053-1583/aa5476
31. Zhang W, Xu H, Xie F, et al. General synthesis of ultrafine metal oxide/reduced graphene oxide nanocomposites for ultrahigh-flux nanofiltration membrane. *Nat Commun*. 2022;13(1):471. doi:10.1038/s41467-022-28180-4
32. Itoo AM, Vemula SL, Gupta MT, et al. Multifunctional graphene oxide nanoparticles for drug delivery in cancer. *J Control Release*. 2022;350:26–59. doi:10.1016/j.jconrel.2022.08.011
33. Sontakke AD, Tiwari S, Purkait MK. A comprehensive review on graphene oxide-based nanocarriers: synthesis, functionalization and biomedical applications. *FlatChem*. 2023;13:100484. doi:10.1016/j.flatc.2023.100484
34. Deng Z, Liu T, Chen T, et al. Enhanced electrochemical performances of Bi2O3/rGO nanocomposite via chemical bonding as anode materials for lithium-ion batteries. *ACS Appl Mater Interfaces*. 2017;9(14):12469–12477. doi:10.1021/acsami.7b00996
35. Mbam SM, Obodo RM, Apeh OO, et al. Performance evaluation of Bi_2O_3@GO and Bi_2O_3@rGO composites electrode for supercapacitor application. *J Mater Sci Mater Electron*. 2023;34(18):1405. doi:10.1007/s10854-023-10835-7
36. Nethravathi PC, Manjula MV, Devaraja S, Sakar M, Suresh D. Eco-friendly preparation of Bi_2O_3, Ag-Bi_2O_3 and Ag-Bi_2O_3-rGO nanomaterials and their photocatalytic H2 evolution, dye degradation, nitrite sensing and biological applications. *J Photochem Photobiol*. 2023;435:114295. doi:10.1016/j.jphotochem.2022.114295

37. Oberdörster G, Oberdörster E, Oberdörster J. Nanotoxicology: an emerging discipline evolving from studies of ultrafine particles. *Environ Health Perspect*. 2005;113(7):823–839. doi:10.1289/ehp.7339
38. Li L, Shen Y, Tang Z, et al. Engineered nanodrug targeting oxidative stress for treatment of acute kidney injury. *Exploration*. 2023;3(6):20220148. doi:10.1002/EXP.20220148
39. Iavicoli I, Fontana L, Nordberg G. The effects of nanoparticles on the renal system. *Crit Rev Toxicol*. 2016;46(6):490–560. doi:10.1080/10408444.2016.1181047
40. Nosrati H, Khodaei M, Alizadeh Z, Banitalebi-Dehkordi M. Cationic, anionic and neutral polysaccharides for skin tissue engineering and wound healing applications. *Int J Biol Macromol*. 2021;192:298–322. doi:10.1016/j.ijbiomac.2021.10.013
41. Dev I, Pal S, Lugun O, Singh N, Ansari KM. Ochratoxin A treated rat derived urinary exosomes enhanced cell growth and extracellular matrix production in normal kidney cells through modulation of TGF-β1/smad2/3 signaling pathway. *Life Sci*. 2022;298:120506. doi:10.1016/j.lfs.2022.120506
42. Lateef R, Mandal P, Ansari KM, Akhtar MJ, Ahamed M, Ahamed M. Cytotoxicity and apoptosis induction of copper oxide-reduced graphene oxide nanocomposites in normal rat kidney cells. *J King Saud Univ Sci*. 2023;35(2):102513. doi:10.1016/j.jksus.2022.102513
43. Piret JP, Jacques D, Audinot JN, et al. Copper (II) oxide nanoparticles penetrate into HepG2 cells, exert cytotoxicity via oxidative stress and induce pro-inflammatory response. *Nanoscale*. 2012;4(22):7168–7184. doi:10.1039/C2NR31785K
44. Siddiqui MA, Ahmad J, Farshori NN, et al. Rotenone-induced oxidative stress and apoptosis in human liver HepG2 cells. *Mol Cell Biochem*. 2013;384:59–69. doi:10.1007/s11010-013-1781-9
45. Mossmann T. Rapid colorimetric assay for cellular growth and survival: application to proliferation and cytotoxicity assays. *J Immunol Methods*. 1983;65(1–2):55–63. doi:10.1016/0022-1759(83)90303-4
46. Ahamed M, Akhtar MJ, Khan MM, Alhadlaq HA. Reduced graphene oxide mitigates cadmium-induced cytotoxicity and oxidative stress in HepG2 cells. *Food Chem Toxicol*. 2020;143:111515. doi:10.1016/j.fct.2020.111515
47. Wang H, Joseph JA. Quantifying cellular oxidative stress by dichlorofluorescein assay using microplate reader. *Free Radic Biol Med*. 1999;27(5–6):612–616. doi:10.1016/S0891-5849(99)00107-0
48. Cury-Boaventura MF, Pompéia C, Curi R. Comparative toxicity of oleic acid and linoleic acid on Jurkat cells. *Clin Nutr*. 2004;23(4):721–732. doi:10.1016/j.clnu.2003.12.004
49. Ahmad J, Alhadlaq HA, Alshamsan A, et al. Differential cytotoxicity of copper ferrite nanoparticles in different human cells. *J Appl Toxicol*. 2016;36(10):1284–1293. doi:10.1002/jat.3299
50. Ellman GL. Tissue sulfhydryl groups. *Arch Biochem Biophys*. 1959;82(1):70–77. doi:10.1016/0003-9861(59)90090-6
51. Bradford MM. A rapid and sensitive method for the quantitation of microgram quantities of protein utilizing the principle of protein-dye binding. *Anal Biochem*. 1976;72:248–254. doi:10.1016/0003-2697(76)90527-3
52. Khan ZR, Khan MT, Shkir M. Improved electrical carrier dynamics and UV detection performance of Zn1-xWxO nanostructured thin films. *Surf Interfaces*. 2023;42:103455. doi:10.1016/j.surfin.2023.103455
53. Zhu G, Yang W, Lv W, et al. Facile electrophoretic deposition of functionalized Bi_2O_3 nanoparticles. *Mater Des*. 2017;116:359–364. doi:10.1016/j.matdes.2016.12.031
54. Alaizeri ZM, Alhadlaq HA, Aldawood S, Akhtar MJ, Ahamed M. Bi_2O_3-Doped WO_3 nanoparticles decorated on rGO sheets: simple synthesis, characterization, photocatalytic performance, and selective cytotoxicity toward human cancer cells. *ACS Omega*. 2023;8(28):25020–25033. doi:10.1021/acsomega.3c01644
55. Ngidi NP, Muchuweni E, Nyamori VO. Synthesis and characterisation of heteroatom-doped reduced graphene oxide/bismuth oxide nanocomposites and their application as photoanodes in DSSCs. *RSC Adv*. 2022;12(4):2462–2472. doi:10.1039/D1RA08888B
56. Caputo F, Clogston J, Calzolai L, Rösslein M, Prina-Mello A. Measuring particle size distribution of nanoparticle enabled medicinal products, the joint view of EUNCL and NCI-NCL. A step-by-step approach combining orthogonal measurements with increasing complexity. *J Control Release*. 2019;299:31–43. doi:10.1016/j.jconrel.2019.02.030
57. Mahmoud NN, Albasha A, Hikmat S, et al. Nanoparticle size and chemical modification play a crucial role in the interaction of nano gold with the brain: extent of accumulation and toxicity. *Biomater Sci*. 2020;8(6):1669–1682. doi:10.1039/C9BM02072A
58. Anushya SA, Prabhu S, Ravikumar V, Philominal A. Screening of anti-cancer activity of rGO–Bi_2O_3 nanocomposite on apoptosis in A549 and NCI-H460 lung cancer cell lines. *J Inorg Organomet Polym Mater*. 2023;33(5):1369–1380. doi:10.1007/s10904-023-02595-y
59. Li D, Muller MB, Gilje S, Kaner RB, Wallace GG. Processable aqueous dispersions of graphene nanosheets. *Nat Nanotechnol*. 2008;3:101–105. doi:10.1038/nnano.2007.451
60. Lee JY, Maeng S, Kang SR, et al. Valproic acid protects motor neuron death by inhibiting oxidative stress and endoplasmic reticulum stress-mediated cytochrome C release after spinal cord injury. *J Neurotrauma*. 2014;31(6):582–594. doi:10.1089/neu.2013.3146
61. Fahmy HM, Ebrahim NM, Gaber MH. In-vitro evaluation of copper/copper oxide nanoparticles cytotoxicity and genotoxicity in normal and cancer lung cell lines. *J Trace Elem Med Biol*. 2020;60:126481. doi:10.1016/j.jtemb.2020.126481
62. Abdelazeim SA, Shehata NI, Aly HF, Shams SG. Amelioration of oxidative stress-mediated apoptosis in copper oxide nanoparticles-induced liver injury in rats by potent antioxidants. *Sci Rep*. 2020;10(1):10812. doi:10.1038/s41598-020-67784-y
63. Sárközy M, Kovács ZZ, Kovács MG, Gáspár R, Szűcs G, Dux L. Mechanisms and modulation of oxidative/nitrative stress in type 4 cardio-renal syndrome and renal sarcopenia. *Front Physiol*. 2018;9:1648. doi:10.3389/fphys.2018.01648
64. Ahamed M, Akhtar MJ, Khan MAM, Alhadlaq HA. Co-exposure of Bi2O3 nanoparticles and bezo[a]pyrene-enhanced in vitro cytotoxicity of mouse spermatogonia cells. *Environ Sci Pollut Res*. 2021;28:17109–17118. doi:10.1007/s11356-020-12128-6
65. Akhtar MJ, Ahamed M, Alhadlaq H. Bismuth Oxide (Bi_2O_3) Nanoparticles Cause Selective Toxicity in a Human Endothelial (HUVE) Cell Line Compared to Epithelial Cells. *Toxics*. 2023;11(4):343. doi:10.3390/toxics11040343
66. Li Y, Zhang W, Niu J, Chen Y. Mechanism of photogenerated reactive oxygen species and correlation with the antibacterial properties of engineered metal-oxide nanoparticles. *ACS Nano*. 2012;6(6):5164–5173. doi:10.1021/nn300934k
67. Akhtar MJ, Ahamed M, Kumar S, Khan MM, Ahmad J, Alrokayan SA. Zinc oxide nanoparticles selectively induce apoptosis in human cancer cells through reactive oxygen species. *Int J Nanomed*. 2012;7:845–857. doi:10.2147/IJN.S29129
68. He H, Zou Z, Wang B, et al. Copper oxide nanoparticles induce oxidative DNA damage and cell death via copper ion-mediated P38 MAPK activation in vascular endothelial cells. *Int J Nanomed*. 2020;8:3291–3302. doi:10.2147/IJN.S241157

69. Carocho M, Ferreira IC. A review on antioxidants, prooxidants and related controversy: natural and synthetic compounds, screening and analysis methodologies and future perspectives. *Food Chem Toxicol*. 2013;51:15–20. doi:10.1016/j.fct.2012.09.021
70. De Nicola M, Ghibelli L. Glutathione depletion in survival and apoptotic pathways. *Front Pharmacol*. 2014;5:267. doi:10.3389/fphar.2014.00267
71. Salvesen GS. Caspases: opening the boxes and interpreting the arrows. *Cell Death Differ*. 2002;9(1):35. doi:10.1038/sj.cdd.4400963
72. Naz S, Gul A, Zia M. Toxicity of copper oxide nanoparticles: a review study. *IET Nanobiotechnol*. 2020;14(1):1–3. doi:10.1049/iet-nbt.2019.0176
73. Gu Q, Tomaskovic-Crook E, Wallace GG, Crook JM. 3D bioprinting human induced pluripotent stem cell constructs for in situ cell proliferation and successive multilineage differentiation. *Adv Healthc Mater*. 2017;6(17):1700175. doi:10.1002/adhm.201700175
74. Phengchat R, Takata H, Morii K, et al. Calcium ions function as a booster of chromosome condensation. *Sci Rep*. 2016;6:38281. doi:10.1038/srep38281
75. Ali D, Alarifi S, Alkahtani S, Almeer RS. Silver-doped graphene oxide nanocomposite triggers cytotoxicity and apoptosis in human hepatic normal and carcinoma cells. *Int J Nanomed*. 2018;24:5685–5699. doi:10.2147/IJN.S165448
76. Liu K, Liu PC, Liu R, Wu X. Dual AO/EB staining to detect apoptosis in osteosarcoma cells compared with flow cytometry. *Med Sci Monit Basic Res*. 2015;21:15. doi:10.12659/MSMBR.893327
77. Anantharaju PG, Reddy BD, Padukudru MA, Kumari CM, Vimalambike MG, Madhunapantula SV. Naturally occurring benzoic acid derivatives retard cancer cell growth by inhibiting histone deacetylases (HDAC). *Cancer Biol Ther*. 2017;18(7):492–504. doi:10.1080/15384047.2017.1324374
78. Muthukumarasamy R, Majeed S, Danish M, et al. Transactivator of transcription peptide conjugated copper oxide nanoparticles: a nano-warrior against breast cancer-Insights from biosynthesis, characterization, and cellular studies. *J Drug Deliv Sci Technol*. 2023;89:104979. doi:10.1016/j.jddst.2023.104979
79. Huang YW, Cambre M, Lee HJ. The toxicity of nanoparticles depends on multiple molecular and physicochemical mechanisms. *Int J Mol Sci*. 2017;18(12):2702. doi:10.3390/ijms18122702
80. Alzahrani B, Elderdery AY, Alsrhani A, et al. Sodium alginate-encapsulated iron oxide decorated with thymoquinone nanocomposite induces apoptosis in human breast cancer cells via PI3K-Akt-mTOR pathway. *Int J Biol Macromol*. 2023;244:125054. doi:10.1016/j.ijbiomac.2023.125054